A microfluidic study of oil-water separation kinetics

T. Krebs[1,2], C. P. G. H. Schroen[2] & R. M. Boom[2]
[1]*Institute for Sustainable Process Technology, The Netherlands*
[2]*Wageningen University, Food Process Engineering Group, The Netherlands*

Abstract

We present the results of experiments studying droplet coalescence in a dense layer of emulsion droplets using microfluidic circuits. The microfluidic structure allows direct observation of shear-induced collisions and coalescence events between oil droplets dispersed in water. A mineral oil was chosen as the dispersed phase and a 9 wt% NaCl aqueous solution as the continuous phase. We determine the coalescence rate as a function of the droplet velocity and droplet concentration from image sequences measured with a high-speed camera. A trajectory analysis of colliding droplet pairs allows evaluation of the film drainage profile and coalescence time t_c. From the coalescence times obtained for ten thousands of droplet pairs we calculate the coalescence time distributions for each set of experimental parameters, which are the mean droplet approach velocity $\langle v_0 \rangle$ and the mean dispersed phase fraction $\langle \phi \rangle$. We discuss the potential of the procedure for the prediction of emulsion stability in industrial applications.
Keywords: emulsion, microfluidic, coalescence, kinetics, image analysis, droplet, film drainage, petroleum.

1 Introduction

The control of emulsion stability is an important issue in many industrial applications. Our motivation is rooted in the field of crude-oil/water separation which is a key processing step in oil production. In this application, a common way to separate the liquid mixture is by using mechanical devices [1], like gravity settlers, centrifugal separators such as hydrocyclones or in-line swirl elements [2]. A criterion for the successful operation of these separators is

WIT Transactions on Engineering Sciences, Vol 74, © 2012 WIT Press
www.witpress.com, ISSN 1743-3533 (on-line)
doi:10.2495/AFM120381

that the demulsification time of the oil/water mixture must be smaller than the residence time of the fluids in the separator. To recover pure oil and water phases, coalescence between emulsion droplets needs to take place; this coalescence time will depend on the nature of the flow as well as the presence of emulsifying agents. To assess the feasibility of a device to separate a crude-oil/water mixture, the kinetic parameters governing coalescence must be known. This becomes especially important in view of Enhanced Oil Recovery methods that use surfactants, which may lead to the formation of stable emulsions. As the separation typically is performed on the oil rig, a fast and robust method to assess crude-oil/water emulsion stability using lab-scale experiments would be useful, which may aid in separator design for a given produced fluid.

A large number of theoretical and experimental studies on droplet coalescence have been performed until now. Generally, the physical processes determining coalescence are well understood [3,4], but difficult to model, as the solution of the involved equations, such as the Navier-Stokes equations to describe the drainage of continuous phase between the droplets, is only possible numerically [5]. The presence of surfactants causes additional complications due to the introduction of colloidal forces [6] and modification of the interfacial rheology [7]. For these reasons, simplified models are often used [8, 9], which provide the necessary accuracy to reliably predict coalescence only for chemically simple systems, and if the droplet deformation during film drainage is not significant.

Extensive experimental studies on coalescence between isolated droplet pairs colliding in simple shear flow have been performed. The influence of collision geometry [10], viscosity ratio of the liquids [11] and the flow field [12] on the droplet trajectories and coalescence probability was studied. As these methods typically use light microscopy to study droplet interactions, density-matched liquids are employed to avoid movement of droplets out of the focal plane due to buoyancy. In doing this, the choice of liquids is limited to very specific model systems. An experimental route to study coalescence in dilute emulsions is to optically measure the evolution of the droplet size distribution of a sheared emulsion in a rheometer. Both *ex*-situ [13] and *in*-situ [14] droplet size measurements have been reported. In the work of Korobko *et al.* [14], a mean coalescence probability was evaluated from the temporal evolution of the droplet size distribution.

The rate r_{ij} of coalescence between droplets of volume V_i and V_j can be expressed as [15]:

$$r_{ij} = \Theta_{ij} p_{ij} = \Theta_{ij} e^{-\langle t_{ij} \rangle / \langle \tau_{ij} \rangle} \tag{1}$$

In eq. (1), Θ_{ij} and p_{ij} are the collision frequency and coalescence probability; $\langle t_{ij} \rangle$ and $\langle \tau_{ij} \rangle$ are the mean coalescence time and the mean contact time between the two droplets for a given flow and fluid properties. Θ_{ij} can be calculated from $\Theta_{ij} = n_i n_j \sigma_{ij} \Delta v_{ij}$, where n_i and n_j are the concentrations of the droplets, σ_{ij} is the collision cross section, and Δv_{ij} is a characteristic velocity difference between the droplets. From an application point of view, it would be ideal being able to directly measure r_{ij} for a given experimental condition, or to measure $\Theta_{ij}, \langle t_{ij} \rangle$ and $\langle \tau_{ij} \rangle$

independently. Further, the set of r_{ij} measured for a given flow condition and fluid properties may be used as an input parameter in the coalescence rate equations of population balance equation (PBE) models [16]. The PBE are used in multiphase Computational Fluid Dynamics methods to describe the evolution of droplet size distributions in fluid-liquid flows [17].

In this article, we present the results of a microfluidic analysis on droplet coalescence in a dense two-dimensional oil-in-water emulsion without added surfactant. We monitor the interactions in an ensemble of droplets in a collision chamber. We perform a detailed evaluation of the droplet interactions in the microchannel and analyze the trajectories of colliding droplets which allows to calculate the coalescence rates for different flow conditions. Further, we obtain the individual coalescence times for droplet pairs as a function of the initial film drainage velocity of the droplets. From this data, we are able to calculate coalescence time distributions for each set of experimental parameters. We will discuss the potential of the method as a predictive tool for crude-oil/water demulsification kinetics.

2 Experimental section

2.1 Chemicals

The physical properties of the mineral oil at 293 K are density $\rho = 869$ kg m^{-3} and viscosity $\eta = 20.1$ mPa s. The aqueous phase was a 9 wt. % solution of NaCl in water (at 293 K: $\rho = 1063$ kg m^{-3}, $\eta = 1.18$ mPa s). Purified water obtained from a Millipore Milli-Q system (ZMQS 50001) and sodium chloride (ACS reagent, $\geq$ 99%, Sigma Aldrich) were used to prepare the solution. All liquids were degassed before use. The interfacial tension of the oil/brine interface at 293 K was measured to be 11 mN m^{-1}.

2.2 Microfluidic experiments

Custom-designed microfluidic circuits were purchased from Micronit B.V., The Netherlands. The microchips are made from glass and have a rectangular cross-section. Figure 1 displays the layout of the chip. All channels have a depth of 45 μm. The width of the channels is 100 μm, except for the channel in the center of the chip, where the droplets collide. This collision channel has a width of 500 μm and a length of 5 mm. The chip contains four inlet and two outlet sections. For droplet creation T-junctions are used, where the continuous (flow rate q_c) and dispersed phase channels (q_d) intersect. By controlling the flow rate ratio q_c/q_d, the droplet volume and frequency can be controlled for a given T-junction geometry [18, 19]. After formation, the droplets then enter a wider channel, where they undergo collisions and coalesce. In this collision channel the droplets are not spherical, but take on a flattened, disk-like shape. The effective hydraulic diameter d_h of a droplet is given by $d_h = 4A/P$, where A and P are the cross sectional area and the perimeter of the droplet. For a disk-shaped droplet, we obtain

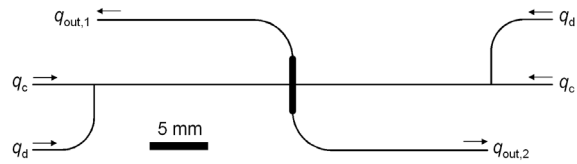

Figure 1: Layout of the microfluidic chips used for the experiments. q_d and q_c denote the inlet sections of the continuous and dispersed phases; $q_{out,1}$ and $q_{out,2}$ denote the outlet sections for the liquids. The channels have a uniform depth of 45 μm, the width of all channels is 100 μm, except for the wider channel in the center of the chip. The width of this channel is 0.5 mm, and the length 5 mm.

$d_h = 4h(d_d - (1-\pi/4)h)/(\pi h + 2(d_d - h))$, where d_d is the diameter of the disk-like droplet and h the channel height. For the flow conditions used in this work, we obtained 70 μm $< d_d <$110 μm, corresponding to 55 μm $< d_h <$ 64 μm.

Before each experiment, the microfluidic chips underwent a cleaning procedure to ensure the hydrophilicity of the channels. First, the channels were filled with an alkaline cleaning solution (Decon 90, Decon Laboratories Ltd.), sonicated for 15 minutes, and afterwards flushed with water. The chips were then blown dry and baked out in an oven for 3 h at 600 °C. Finally, the chips were subjected to an oxygen plasma for 10 minutes (Zepto B Plasma Cleaner, Diener Electronic GmbH).

The microfluidic chips are mounted on a chip holder (4515 Nanoport, Micronit B.V., The Netherlands). The inlet sections of the chips are connected to silica capillary tubing (Grace Altech, inner diameter 150 μm). The liquids are dosed using syringe pumps (NE 1000, New Era Pump Systems, Inc.). The flow rates of dispersed phase q_d at the two different inlets of the dispersed phase were always kept equal, as were the flow rates of continuous phase q_c. This was done to assure identical droplet volumes and formation rates obtained from both T-junctions. The two outlet sections have the same hydraulic resistance. To change the flow rate ratio $q_{out,1}/q_{out,2}$ of the outlet sections, and thus the flow rate ratio in the upper and lower part of the collision channel, capillary tubings of different length (inner diameter 50 μm) were attached to the outlet sections.

The droplet interactions in the collision channel are monitored using a microscope (Axiovert 200 MAT, Carl Zeiss GmbH, 2.5× magnification) and a camera (HS4, IDT Inc.). The frame rate of the recorded movies was 10000 s^{-1}. Sequences of images were recorded from one half-section of the collision channel, thereby sampling an area of 0.5×2 mm^2. Experimental parameters were the continuous and dispersed phase flow rates, q_c and q_d, as well as the outlet flow rates $q_{out,1}$ and $q_{out,2}$. By varying these parameters, the mean drop velocity in the collision chamber v_d and the dispersed volume fraction ϕ can be controlled independently from each other. For each experimental condition, movies with a length of 2 s were recorded (Motion Studio Software, IDT Inc.). The range of

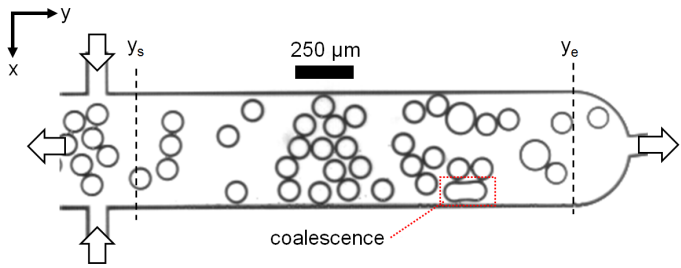

Figure 2: Snapshot of the collision channel. Monodisperse oil droplets ($d_d = 97$ μm in this example) dispersed in the aqueous phase enter the chamber from two inlets, where they collide and coalesce. The total fluid flow rate in the collision channel is 60 μl min^{-1}. y_s and y_e denote the start and end y-coordinate for the evaluation of coalescence events in the chamber. The red dotted rectangle encloses a droplet that was formed through coalescence between the displayed and the previous frame.

experimental parameters was $0.21 < q_d/q_c < 0.71$, 2 μl min^{-1} $< q_t <$ 300μl min^{-1} and 70 μm $< d_d <$ 110 μm. q_t denotes the total fluid flow rate, $q_t = q_c + q_d$.

3 Results and discussion

Figure 2 displays a snapshot of the collision channel during an experiment as an example. Monodisperse oil droplets with $d_d \approx 97$ μm enter the channel from two inlets and then move into the wider channel were they undergo collisions. The flow rate q_{out} in each section of the collision channel in this example is $q_{out} \approx 60$ μl min^{-1}. The flow rate ratio is $q_d/q_c \approx 0.15$, but the dispersed phase fraction ϕ in the collision channel is $\phi \approx 0.29$. This difference is caused by the fact that the disk-shaped droplets in the collision channel will experience a larger drag due to contact with the wall and will thus move significantly slower than the continuous phase. Due to this effect, there will be a holdup of droplets in the collision channel.

The mean droplet size increases as the droplets move downstream in the collision channel. This growth in droplet size is caused by coalescence between colliding droplets, which will lead to droplet sizes in the channel ranging from the original volume of a droplet V_1 entering the chamber, to a droplet volume of $V_i = iV_1$, where $i-1$ indicates the number of coalescence events that led to the formation of the droplet. The collisions are caused by differences in droplet velocity, which originate from local differences in hydraulic resistance caused by the presence of neighboring drops, and from the velocity profile that exists in laminar channel flow.

3.1 Evaluation of the coalescence rate

Counting the number of coalescence events permits to calculate the coalescence rate r_{ij}. We define r_{ij} for a combination of droplets of volume V_i and V_j as

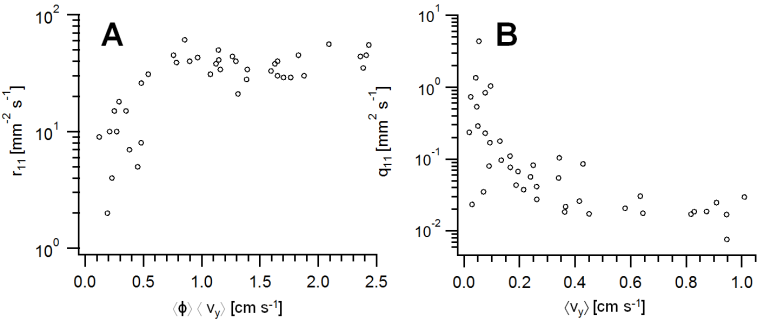

Figure 3: Coalescence rate r_{11} of the oil/brine system for droplets of relative volume $V_i/V_1 = 1$, as a function of the mean dispersed phase flux $\langle\phi\rangle\langle v_y\rangle$ (shown in panel A). $\langle\phi\rangle$ denotes the mean dispersed phase volume fraction and $\langle v_y\rangle$ the mean y-component of the droplet velocity in the collision channel. Panel B displays the specific coalescence rate q_{11} of the oil/brine system as a function of the mean y-component of the droplet velocity $\langle v_y\rangle$ in the collision channel. The mean hydraulic diameter of the droplets entering the collision channel was $d = (58 \pm 4.7)\ \mu$m.

$r_{ij} = n_{c,ij}/A_c t_{exp}$, where $n_{c,ij}$ is the number of coalescence events between droplets i and j, A_c is the area of the collision channel, and t_{exp} the experiment time. The procedure to determine r_{ij} from the image sequences is described elsewhere [20]. Only coalescence events occurring between the y-coordinates y_s and y_e were counted (see Figure 2).

r_{11} is shown in Figure 3A as a function of the mean dispersed phase flux $\langle\phi\rangle\langle v_y\rangle$ in the collision channel. $\langle\phi\rangle$ denotes the mean dispersed phase volume fraction and $\langle v_y\rangle$ the mean y-component of the droplet velocity in the collision channel. The mean hydraulic diameter of the droplets was $(58 \pm 4.7)\ \mu$m. The scatter of the data points is significant, this is caused by the relatively small number of droplets passing through the chamber in 2 s, which ranged from 200–5000, depending on the flow rate. The r_{ij} for $i \geq 1$ and $j > 1$ are not shown. r_{12} was on average approximately one order of magnitude smaller than r_{11} and all other r_{ij} were on average zero.

The measured dependence $r_{11}(\langle\phi\rangle\langle v_y\rangle)$ can be qualitatively explained from equation (1). The mean shear rate $\langle\dot{\gamma}\rangle$ in the microchannel is related to v_y by $\langle\dot{\gamma}\rangle \propto v_y$ [21]. In simple shear, the collision frequency will depend on $\langle\dot{\gamma}\rangle$ as $\Theta_{ij} \propto \dot{\gamma}$ and the coalescence probability $ln(p_{ij}) \propto \dot{\gamma}^{-n}$. Korobko *et al.* found $n = 1.5 \pm 1$ from experiments on coalescence in simple shear flow [14]. The flow in the microfluidic channel is not simple shear flow due to the large dispersed phase fractions, but qualitatively we would expect a similar scaling of the parameters in equation 1 in our system. Depending on the value of n, r_{ij} may increase monotonously or pass through a maximum in a given range of $\dot{\gamma}$.

To account for the effect of droplet concentrations on the coalescence rate, we calculate the specific coalescence rate $q_{11} = r_{11}/\langle n_1\rangle^2$. $\langle n_1\rangle$ is the mean

concentration of droplets with volume V_1 in the collision channel. q_{11} is formally equivalent to a second-order rate constant. Figure 3B displays q_{11} as a function of the mean y-component of droplet velocity $\langle v_y \rangle$ in the collision channel. From eq. (1), the decrease of q_{ij} with v_y indicates a decrease of the coalescence probability p_{ij} with increasing v_y, as Θ_{ij} will increase with increasing $\langle v_y \rangle$.

3.2 Evaluation of the film drainage profiles and coalescence times

If experimental data for q_{ij} is not available, then eq. (1) can, in principle, be used to predict q_{ij}. For turbulent flow and laminar shear flow, analytical relations for the collision frequency Θ_{ij} and contact time τ_{ij} can be derived if the characteristic velocity variation Δv between droplets in the flow is known. For the turbulent flow this property is related to the rate of energy dissipation ε through $\Delta v \propto \varepsilon^{1/3}$ [22]. For laminar shear flow the shear rate $\dot{\gamma}$ will determine the magnitude of Δv, $\dot{\gamma} \propto \Delta v$ [15, 22]. For the coalescence time t_c no general analytical equation can be derived, except for certain idealized situations, which are typically not encountered in applications. Hence, a possible experimental measurement of $t_c(\Delta v)$ can also be useful for coalescence modeling. We argue that the $t_c(\Delta v)$, which we measure, can also be used to describe coalescence in other flow conditions. On a microscopic scale the approach velocity and force will determine the timescale of coalescence, rather than the mechanism which is bringing the droplets together in the flow. In this section, we will derive $t_c(\Delta v)$ from the recorded trajectories of coalescing droplets in the microchannels.

Evaluation of the trajectories of colliding droplets permits to calculate the coalescence time t_c, which we define as the time it takes the droplets to approach each other from a given initial distance h_0 to a critical thickness h_c at which coalescence takes place, i.e. $t_c = \int_{h_0}^{h_c} dh/v_f$. In the equation, $v_f = -dh/dt$ denotes the velocity of drainage of the continuous phase film between the two droplets. Due to the limited spatial resolution of the microscope that was used in the experiments we cannot resolve the film drainage process until h_c is reached, as $h_c < 100$ nm [23]. We can, however, identify a coalescence event. The occurrence of coalescence indicates that $h \leq h_c$ between two recorded frames, thus permitting to calculate $t_c \approx (F(h_0) - F(h_c))/f$, whereas F indicates the frames with the relevant film thicknesses and f indicates the frame rate of the camera.

The inset in Figure 4 schematically displays the geometry of a pair of colliding droplets k and l. The film thickness can be calculated from $h \approx ((x_k - x_l)^2 + (y_k - y_l)^2 - (r_k + r_l))^{1/2}$. In doing this, a spherical shape of the droplets is assumed. The validity of this assumption was checked by evaluation of the circularity parameter $c = 4\pi A/P^2$. For circular objects, $c = 1$. It was found that for $\sim 90\%$ of all analyzed droplets c was > 0.95, which indicated circular or almost circular shape of the droplets. Droplets for which $c < 0.95$ were discarded from the analysis.

As long as the droplets are still visibly separated, the drag force on a droplet will be balanced by the force exerted by the flow. Thus, we can calculate a relative initial approach or film thinning velocity of the droplets along the line connecting

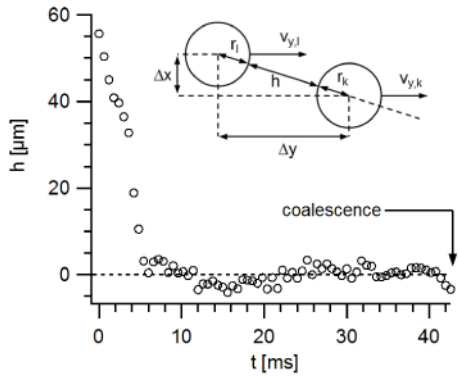

Figure 4: Film drainage profile $h(t)$ of two colliding droplets k and l. The droplets approach each other, spend time in close contact and then coalesce. The end of the curve at $t = 42.4$ ms marks the time when coalescence takes place. The initial film thickness ($h_0 = d_h/8 \approx 7\ \mu$m in this example) is reached after 4.4 ms, thus a coalescence time $t_c = 38$ ms is obtained. The mean initial approach velocity v_0, which was evaluated in the interval 0–4.4 ms, is ≈ 9.4 mm s^{-1} in this example. The inset shows the collision geometry. $\Delta x = x_k - x_l$ and $\Delta y = y_k - y_l$ signify the difference of the x- and y- coordinates of the centers of mass of the droplets, respectively. r_l and r_k are the droplet radii, h is the thickness of the film of continuous phase between the droplets. $v_{y,k}$ and $v_{y,l}$ are the velocity components of the droplets parallel to the downstream channel direction.

their center of mass $v_0 = -dh/dt$. From all the videos recorded for different flow conditions and dispersed phase fractions, the coalescence time of colliding droplets was evaluated. Only droplet pairs for which the initial separation distance was $\geq 30\ \mu$m were considered, in order to obtain enough data points to calculate v_0. v_0 was calculated for each droplet pair as a mean value $\langle \Delta h/\Delta t \rangle$ in the interval $h_0 < h < 30\ \mu$m, whereas $h_0 = d_h/8$, which is an estimate for the film thickness at which the film drainage rate becomes smaller than the shear-induced velocity bringing the droplets together [7]. The coalescence time was then calculated using the same definition of h_0 for the initial film thickness.

From all recorded videos, a total of $\sim$ 10000 film drainage profiles fulfilled the aforementioned criteria for evaluation. To each data point also a hydraulic droplet diameter d_h and a dispersed phase volume fraction ϕ are assigned. Visual inspection of the data set indicated that there was a distribution of coalescence times for a given v_0. These coalescence time distributions may depend on ϕ and d_h in addition to the dependence on v_0. As the range of d_h was relatively small (55–64 μm), the dependence $t_c(d_h)$ was not investigated. To evaluate the dependence $t_c(\phi)$ we sort the data into 5 bins of different ranges of ϕ with equal amounts of data points. For the dependence $t_c(v_0)$ for a given $\langle \phi \rangle_i$, we further sort a given set of data points of bin i into 5 bins of ascending v_0 and calculate the

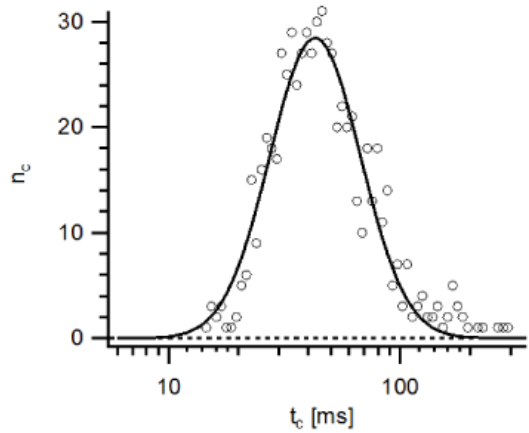

Figure 5: Distribution of coalescence times $n_c(t_c)$ for $\langle\phi\rangle$ = 0.61 ± 0.087 and $\langle v_0\rangle = (5.8 \pm 1.1)$ mm s^{-1}. The mean hydraulic diameter of the colliding droplets was (54 ± 4.7) μm. The solid line is a log normal distribution which was fitted to the data points. The expected value E_{t_c} of this data set is 53 ms.

distribution of coalescence times for each bin. The upper and lower boundaries of the v_0 bins were chosen in a way to obtain the same geometric mean $\langle v_0\rangle_j$ for different $\langle\phi\rangle_i$, to allow a better comparison of the results. Figure 5 displays the distribution of coalescence events $n_c(t_c)$ for the bin with $\langle\phi\rangle_i = 0.61 \pm 0.087$ and $\langle v_0\rangle = 5.8 \pm 1.1$ mm s^{-1} as an example. It was found that all $n_c(t_c)$ distributions calculated in this way could be well described by log normal distributions:

$$n_c(t_c) \propto \frac{1}{\sqrt{2\pi}t_c\sigma} e^{-\frac{(lnt_c-\mu)^2}{2\sigma^2}} \tag{2}$$

The expected value E_{t_c} and standard deviation σ_{t_c} of the distribution can be calculated from the parameters μ and σ, $E_{t_c} = e^{\mu+0.5\sigma^2}$ and $\sigma_{t_c} = E_{t_c}\sqrt{e^{\sigma^2}-1}$. From all the distributions obtained for the different $\langle\phi\rangle_i$ and $\langle v_0\rangle_j$ bins, we evaluate E_{t_c} and σ_{t_c}. E_{t_c} is shown in Figure 6 as a function of $\langle v_0\rangle$ for the different $\langle\phi\rangle_i$. It can be seen that E_{t_c} decreases weakly with increasing $\langle v_0\rangle$. From power law fits to the data series, we obtain $E_{t_c} = (31.7 \pm 2.8) \times 10^{-3}\langle v_0\rangle^{-0.097\pm0.012}$. Hydrodynamical theory predicts $t_c \propto \dot{\gamma}^{-0.5}$ in the limit of $Ca = \eta_c d_h \dot{\gamma}/\sigma \to 0$ [12], and an increase of the exponent −0.5 to a maximum value of 0.5 for $Ca \to \infty$ [7]. We can calculate a local shear rate of colliding droplets for our experiments from $\dot{\gamma}_{kl} = (v_{y,l} - v_{y,k})/(|\, x_l - x_k \,|)$ (see Figure 4). From plotting E_{t_c} vs. $\langle\dot{\gamma}_{kl}\rangle$ we obtain $E_{t_c} = (37.6 \pm 2.7) \times 10^{-2}\langle\dot{\gamma}_{kl}\rangle^{-0.067\pm0.009}$ from a power law fit to the data points. The range of 10^{-3} m s$^{-1} < v_0 < 10^{-1}$ m s^{-1} corresponds approximately to a range of shear rates 1 s$^{-1} < \dot{\gamma}_{kl} < 1000$ s^{-1}. The exponent of -0.067 found by us for our experimental system thus lies within the range of theoretically possible values.

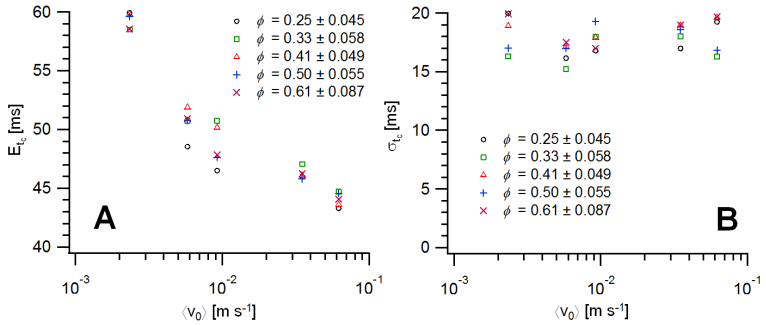

Figure 6: Expected values E_{t_c} (panel A) and standard deviations σ_{t_c} (panel B) of the coalescence time distributions as a function of the mean initial approach velocity $\langle v_0 \rangle$ for different mean dispersed phase fractions $\langle \phi \rangle_i$.

There is no trend of t_c for the different $\langle \phi \rangle_i$ for a given $\langle v_0 \rangle$, which indicates that the presence or absence of neighboring droplets does not modify the average coalescence time. Panel B of Figure 6 displays σ_{t_c} as a function of $\langle v_0 \rangle$ for the different $\langle \phi \rangle_i$. Neither a clear trend of σ_{t_c} as a function of $\langle v_0 \rangle$ and $\langle \phi \rangle_i$ can be observed. Thus we can conclude that the presence of neighboring droplets also does not lead to a broadening of the coalescence time distributions.

Even though we do not know why the coalescence time distribution can be described by a log-normal distribution, we think that the major reason for the existence of a rather wide distribution is that the droplets are moving in an external flow field. During the collision, the leading droplet will induce a wake which will effect the drag force acting on the trailing droplet [24]. Depending on the magnitude of the absolute velocities of the droplets and the collision angle, the wake effect can cause a net attraction or repulsion of the droplets [25]. The magnitude of the effect increases with decreasing h. Further, as the droplets are subjected to shear flow, droplet deformation during the collision can be expected to be asymmetrical. These factors will influence the timescale of film drainage and magnitude of droplet deformation. Additionally, the critical film thickness itself in a quiescent emulsion has a probability distribution, which contributes to the observed coalescence time distribution [3, 8].

4 Conclusions and outlook

We have presented a method to evaluate the demulsification kinetics of liquid-liquid mixtures. The coalescence rate in a hexadecane-in-water emulsion without added surfactant was measured, which is a parameter that has been difficult to obtain directly until now. Due to the simplicity of the experimental setup and the evaluation procedure, the method provides an easy-to-use diagnostic tool for the assessment of the stability of flowing dispersions. As the flow rates can be adjusted quickly, a complete set of coalescence parameters can be obtained as a function of the experimental variables d, ϕ and q_t within a few hours.

In the current design, the method is best suited for the investigation of oil-in-water emulsions. For crude-oil-production, the breakup of water-in-oil emulsions is equally important. When using glass chips, the channels can be made temporarily hydrophobic in a simple manner by adsorption of alkylsilanes on the glass surface for the duration of an experiment [26], to enable the formation of water droplets. Alternatively, the microstructures can be made from hydrophobic materials [27].

The measured coalescence times are smaller than the residence times of the droplets in the collision channels, which in our experiments ranged from 0.1 to 2 seconds, depending on the fluid flow rate. If the viscosity of the continuous phase is increased, or surfactant is present in the system, then the coalescence time will be increased [8]. For these systems, the length of the collision channel can be increased to increase the residence time of the droplets.

The range of accessible hydraulic diameters is currently limited due to the droplet being squeezed into a disk-like shape in the collision channel. This issue may be solved by producing microstructures with a non-uniform depth, where the height of the collision channel will be several times larger than the height of the T-junction. This will allow the droplet to take on a spherical shape, thus increasing its hydraulic diameter.

Acknowledgement

This work is carried out as part of a project of the Institute for Sustainable Process Technology: development of an Ω^2R separator focusing on oil/water separation (project number OG 00-04).

References

[1] Lyons, W., *Standard Handbook of Petroleum and Natural Gas Engineering*. Elsevier, 2nd edition, 2004.
[2] Slot, J., Van Campen, L., Hoeijmakers, H. & Mudde, R., Separation of oil droplets in swirling water flow. *7th International Conference on Multiphase Flow - ICMF 2010 Proceedings*, p. 11.4.2, 2010.
[3] Walstra, P., *Physical Chemistry of Foods*. Marcel Dekker, 1st edition, 2003.
[4] Sjöblom, J., (ed.) *Encyclopedic Handbook of Emulsion Technology*. Marcel Dekker, 1st edition, 2001.
[5] Hartland, S., Yang, B. & Jeelani, S., Dimple formation in the thin film beneath a drop or bubble approaching a plane surface. *Chem Eng Sci*, **49(9)**, pp. 1313–1322, 1994.
[6] Danov, K., Petsev, D. & Denkov, D., Pair interaction energy between deformable drops and bubbles. *J Chem Phys*, **99(9)**, pp. 7179–7189, 1993.
[7] Chesters, A. & Bazhlekov, I., Effect of insoluble surfactants on drainage and rupture of a film between drops interacting under a constant force. *J Colloid Interf Sci*, **230**, pp. 229–243, 2000.
[8] Ivanov, I., Danov, K. & Kralchevsky, P., Flocculation and coalescence of micron-size emulsion droplets. *Colloid Surface A*, **152**, pp. 161–182, 1999.

[9] Rommel, W., Meon, W. & Blass, E., Hydrodynamic modeling of droplet coalescence at liquid-liquid interfaces. *Separ Sci Technol*, **27(2)**, pp. 129–159, 1992.
[10] Guido, S. & Simeone, M., Binary collision of drops in simple shear flow bycomputer-assisted video optical microscopy. *J Fluid Mech*, **357**, pp. 1–20, 1998.
[11] Baldessari, F. & Leal, G., Effect of overall drop deformation on flow-induced coalescence at low capillary numbers. *Phys Fluids*, **18**, pp. 013602 1–20, 2006.
[12] Yang, H., Park, C., Hu, Y. & Leal, L., The coalescence of two equal-sized drops in a two-dimensional linear flow. *Physics of Fluids*, **13**, pp. 1087–1106, 2001.
[13] Nandi, A., Mehra, A. & Khakhar, D., Coalescence in a surfactant-less emulsion under simple shear flow. *AIChE J*, **52(3)**, pp. 885–894, 2006.
[14] Korobko, A., Van Den Ende, D., Agterof, W. & Mellema, J., Coalescence in semiconcentrated emulsions in simple shear flow. *J Chem Phys*, **123**, pp. 204908 1–11, 2005.
[15] Prince, M. & Blanch, H., Bubble coalescence and break-up in air-sparged bubble columns. *AIChe J*, **36**, pp. 1485–1499, 1990.
[16] Schütz, S., Gorbach, G. & Piesche, M., Modeling fluid behavior and droplet interactions during liquid-liquid separation in hydrocyclones. *Chem Eng Sci*, **64**, pp. 3935–3952, 2009.
[17] Ansys cfx user manual. http://www1.ansys.com/customer/content/documentation/120/cfx/xthry.pdf.
[18] Christopher, G. & Anna, S., Microfluidic methods for generating continuous droplet streams. *J Phys D Appl Phys*, **40**, pp. R319–R336, 2007.
[19] Garstecki, P., Fuerstman, M., Stone, H. & Whitesides, G., Formation of droplets and bubbles in a microfluidic t-junction - scaling and mechanism of break-up. *Lab Chip*, **6**, pp. 437–446, 2006.
[20] Krebs, T., Schroen, C. & Boom, R., to be submitted for publication.
[21] Bruus, H., *Theoretical Microfluidics*. Oxford University Press, 1st edition, 2008.
[22] Chesters, A., The modelling of coalescence processes in fluid-liquid dispersions: A review of current understanding. *Trans IChemE*, **69A**, pp. 259–270, 1991.
[23] Birdi, K., *Handbook of Surface and Colloid Chemistry*. CRC Press, 2nd edition, 2003.
[24] Happel, J. & Brenner, H., *Low Reynolds Number Hydrodynamics: With Special Applications to Particulate Media*. Prentice-Hall, 1st edition, 1965.
[25] Hallez, Y. & Legendre, D., Interaction between two spherical bubbles rising in a viscous liquid. *Journal of Fluid Mechanics*, **673**, pp. 406–431, 2011.
[26] Butt, H., Graf, K. & Kappl, M., *Physics and Chemistry of Interfaces*. Wiley VCH, 1st edition, 2003.
[27] Xia, Y. & Whitesides, G., Soft lithography. *Annual Reviews in Material Science*, **28**, pp. 153–184, 1998.